applied optics

Using a unique mirror to minimize the effect of ruling engine cosine error on grating performance

Xiaotao Mi,[1] Shanwen Zhang,[1] Hongzhu Yu,[1,*] Haili Yu,[1] Min Cong,[1,2] and Xiangdong Qi[1]

[1]Changchun Institute of Optics, Fine Mechanics and Physics, Chinese Academy of Sciences, Changchun Jilin 130033, China
[2]University of Chinese Academy of Sciences, Beijing 100049, China
*Corresponding author: yhz_jl@sina.com

Received 10 September 2018; revised 6 November 2018; accepted 6 November 2018; posted 6 November 2018 (Doc. ID 345442); published 4 December 2018

The cosine error of the diffraction grating ruling engine is a systematic error caused by the measurement system. This error affects grating performance directly. To reduce the effects of the cosine error on grating performance, we analyze the cause of the cosine error, establish a mathematical model based on the error and the related grating indicators, and propose a method to reduce the error. To validate the proposed method, we present the results of grating ruling experiments performed before and after cosine error correction, which show that the method effectively reduces the cosine error effects.

https://doi.org/10.1364/AO.57.010146

1. INTRODUCTION

The excellence of grating functions such as dispersion, polarization, and phase matching have led to strong demand for these elements, and particularly for high-quality and large-sized gratings in fields ranging from astronomy to biochemical analysis, military, and aerospace applications [1–5]. The mechanical ruling method, which is one of the most important methods for grating production, is mainly used to produce gratings with deep grooves and strictly defined shapes, such as echelle gratings [6,7].

The diffraction grating ruling engine is essential for grating fabrication when using the mechanical ruling method. In all early ruling engines, and in many of the later engines, the positioning of the grooves and the quality of the gratings were dependent on the mechanical accuracy of the component parts and the assembly accuracy of the entire engine. Considerable efforts have been made to improve the positioning accuracy of the ruling engine. However, the fundamental factors that limit the precision of the ruling engine are material properties such as its stiffness and stability [8–15]. In the 1950s, the physicists Harrison and Stroke put Michelson's proposal of a servo system controlled using an interferometer into practice; the positions of the grating grooves were then determined based on the wavelength of the light, and the grating performance, in terms of problems such as ghosts and light scattering, improved greatly [16]. Internationally, the interference servo control system is used in well-known ruling engines such as the MIT-C engine, which is currently the largest ruling engine in the world and has the ability to rule blanks with dimensions of up to 450 mm × 650 mm × 125 mm, and the Hitachi-4 engine, which has ruled gratings with 10,000 grooves/mm [17–19].

However, the introduction of interferometric systems is likely to bring new errors, such as the cosine error and the Abbe error, which are associated with the beam path structure, and errors caused by refractive index changes, which will affect the accuracy of groove positioning and overall grating performance. In this paper, based on the characteristics of the beam path structure of the measurement system used for the CIOMP-6 ruling engine, we analyze the causes of the cosine error and establish a mathematical model of the cosine error and its related indicators. We then propose a method to reduce the cosine error, and the proposed method is shown to be effective via the results of grating ruling experiments.

2. COSINE ERROR OF THE CIOMP-6 RULING ENGINE

The CIOMP-6 ruling engine, which offers travel of 680 mm, is fitted to rule blanks with dimensions of up to 400 mm × 500 mm × 100 mm. The carriage yaw during a 680 mm traverse was measured using a collimator to be 0.03 s of arc, which will cause fanning in 400-mm-long grooves. The CIOMP-6 ruling engine uses dual-frequency laser interferometers as measurement instruments. To measure the yaw error of the carriage during the grating ruling process, the beam path structure that we designed is as shown in Fig. 1. As the figure shows, the beam from the laser is separated into two beams using a beam splitter; one beam is received at receptor A after passing through interferometer A and mirror A, while the other is received at receptor B after passing through a beam bender, interferometer B, and mirror B. Because of the presence of the carriage yaw error, the carriage displacement measured by one interferometer is

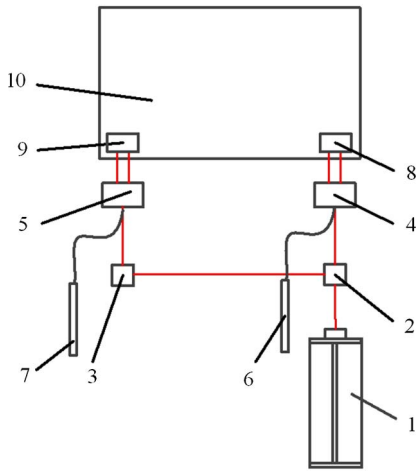

Fig. 1. Beam path structure of the measurement system. 1, laser; 2, beam splitter; 3, beam bender; 4, interferometer A; 5, interferometer B; 6, receptor A; 7, receptor B; 8, mirror A; 9, mirror B; 10, insider carriage.

not the same as that measured by the other. As shown in Fig. 2, the carriage yaw error at the measurement position is given by

$$\theta = \arctan\left(\frac{l_1 - l_2}{a}\right). \tag{1}$$

Here, l_1 is the carriage displacement as measured using interferometer A, l_2 is the carriage displacement as measured using interferometer B, and a (420 mm) is the distance between the axes of the two measuring beams.

The cosine error of the CIOMP-6 ruling engine is a result of angular misalignment between the motion direction of the blank carriage and the laser interferometer beam path. When the beam path is adjusted, we hope that the position of the laser spot on the measuring mirror does not shift with the movement of the blank carriage. However, it is difficult for the human eye to distinguish whether the position of the laser spot has moved because the diameter of laser spot is 3 mm, significantly larger than the potential motion of the spot. In the existing measurement system, mirrors are used in both beam paths, the two beam paths are adjusted separately, and the cosine error angles shown in Fig. 3 then likely appear. In Fig. 3, α_1 and α_2 represent the cosine error angles in beam path 1 and beam path 2, respectively, the displacements measured using the two interferometers are d_1 and d_2, and the actual displacements of the carriage, denoted by d_1' and d_2', are calculated as follows:

$$\begin{cases} d_1' = d_1 \cdot \cos\alpha_1 \\ d_2' = d_2 \cdot \cos\alpha_2 \end{cases}. \tag{2}$$

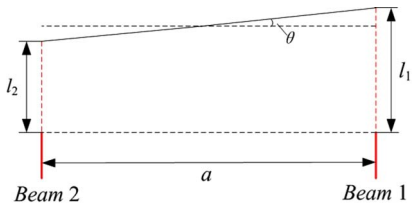

Fig. 2. Measurement of yaw error.

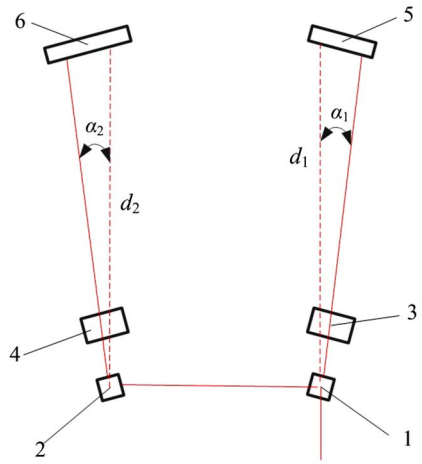

Fig. 3. Cosine error angles of the two beams. 1, beam splitter; 2, beam bender; 3, interferometer A; 4, interferometer B; 5, mirror A; 6, mirror B.

The deviations between the measured displacements and the actual displacements (i.e., the cosine errors) are given by

$$\begin{cases} \Delta d_1 = d_1 - d_1' = d_1 \cdot (1 - \cos\alpha_1) = d_1 \cdot \frac{\alpha_1^2}{2} \\ \Delta d_2 = d_2 - d_2' = d_2 \cdot (1 - \cos\alpha_2) = d_2 \cdot \frac{\alpha_2^2}{2} \end{cases}. \tag{3}$$

It can be found from the above formula that the value of each cosine error is proportional to the displacement when the cosine error angle remains constant. The cosine errors between any two grooves can then be obtained as follows:

$$\begin{cases} \zeta_1 = (d_i - d_{i-1}) \cdot \frac{\alpha_1^2}{2} = d \cdot \frac{\alpha_1^2}{2} \\ \zeta_2 = (d_i - d_{i-1}) \cdot \frac{\alpha_2^2}{2} = d \cdot \frac{\alpha_2^2}{2} \end{cases}. \tag{4}$$

Here, d_i is the measurement position of the ith groove, d_{i-1} is the measurement position of the $(i-1)$th groove, and d is the grating constant.

3. MATHEMATICAL MODEL OF THE COSINE ERROR AND THE RELATED INDICATORS OF THE GRATING

The CIOMP-6 engine uses stop-and-go blank motion, where the carriage remains stationary during the grating ruling process. As indicated in the above analysis, the cosine error will produce a groove error as shown in Fig. 4, where this groove error has the following characteristics:

(1) The spacing between any two adjacent grooves at the same ruling position has the same value.

(2) The spacing between two adjacent grooves changes linearly along the ruling direction.

(3) At the same ruling position in different grooves, the deviation between actual position and theoretical position increases with increasing groove number n, the amount of each increase is constant, and its value is given by the difference between the spacing of two adjacent grooves at the ruling position and the grating constant.

The effect of the cosine error on the grating performance can be divided into two cases.

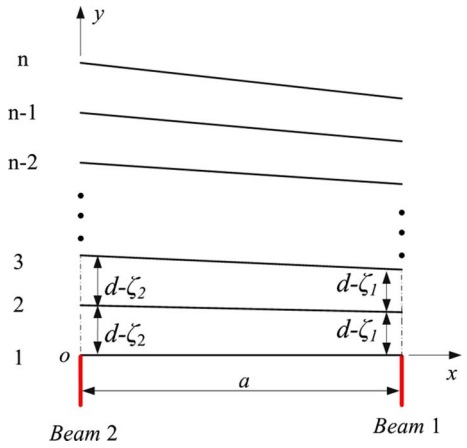

Fig. 4. Schematic diagram of groove error caused by cosine error.

A. If $\alpha_1 = \alpha_2$

From Eq. (4), if $\alpha_1 = \alpha_2$, then occurrence of the cosine error will only lead to changes in the grating constant. Given that the grating constant is the reciprocal of the grating's groove density, the change in the groove density can be given by

$$\Delta\rho = \frac{1}{d-\delta} - \frac{1}{d} = \frac{1}{d - d\cdot\frac{\alpha^2}{2}} - \frac{1}{d} = \frac{1}{d}\cdot\left(\frac{\frac{\alpha^2}{2}}{1-\frac{\alpha^2}{2}}\right) = \rho\cdot\left(\frac{\frac{\alpha^2}{2}}{1-\frac{\alpha^2}{2}}\right), \tag{5}$$

where $\Delta\rho$ is the change in the groove density, and ρ is the grating groove density.

It can be determined from Eq. (5) that the change in the groove density is proportional to the grating groove density when the cosine error angle remains constant.

The carriage travel is 680 mm, and the laser spot diameter is 3 mm. Consider the following bad situation, where we assume that the deviation of the spot's center during a 680 mm traverse is found to be 1.5 mm after beam adjustment, which means that the cosine error angle can be written as

$$\alpha = \arcsin\left(\frac{1.5}{680}\right) = 0.1264°. \tag{6}$$

Combining Eqs. (5) and (6) allows the change in the groove density to be given as

$$\Delta\rho = \rho\cdot\left(\frac{\frac{\alpha^2}{2}}{1-\frac{\alpha^2}{2}}\right) = 2.433\times10^{-6}\cdot\rho. \tag{7}$$

As Eq. (7) shows, the cosine error has a very small effect on the changes in the groove density, and its influence on the grating performance can thus be neglected.

B. If $\alpha_1 \neq \alpha_2$

From Eq. (4) and Fig. 4, if $\alpha_1 \neq \alpha_2$, the cosine error will then cause the grating groove density to vary at different positions in the groove.

It can be deduced from Eq. (4) that the groove error at different positions within the same two adjacent grooves can be written as

$$\zeta(j) = \frac{\zeta_1 - \zeta_2}{m-1}\cdot j + \zeta_2, \qquad (j = 0, 1, 2, \ldots, m-1), \tag{8}$$

where m is the number of sampling points.

For a monolithic grating, the groove error can be expressed as

$$\boldsymbol{\delta}_{nm} = \begin{bmatrix} \delta_{11} & \delta_{21} & \cdots & \delta_{n1} \\ \delta_{12} & \delta_{22} & \cdots & \delta_{n2} \\ \vdots & \vdots & \vdots & \vdots \\ \delta_{1m} & \delta_{2m} & \cdots & \delta_{nm} \end{bmatrix}, \tag{9}$$

where n is the total number of grooves in the grating.

Equations (8) and (9) can be combined so that the groove error matrix can be written as

$$\boldsymbol{\delta}_{\mathrm{nm}} = \begin{bmatrix} 0 & \zeta_2 & \cdots & (n-1)\cdot\zeta_2 \\ 0 & \zeta_2 + \frac{\zeta_1-\zeta_2}{m-1} & \cdots & \zeta_2 + (n-1)\cdot\frac{\zeta_1-\zeta_2}{m-1} \\ \vdots & \vdots & \cdots & \vdots \\ 0 & \zeta_2 + \frac{\zeta_1-\zeta_2}{m-1}\cdot(j-1) & \cdots & \zeta_2 + (n-1)\cdot\frac{\zeta_1-\zeta_2}{m-1}\cdot(j-1) \\ \vdots & \vdots & \cdots & \vdots \\ 0 & \zeta_2 + \frac{\zeta_1-\zeta_2}{m-1}\cdot(m-1) & \cdots & \zeta_2 + (n-1)\cdot\frac{\zeta_1-\zeta_2}{m-1}\cdot(m-1) \end{bmatrix}. \tag{10}$$

As shown in Fig. 5, the sign conventions for the angles and diffraction orders are as follows:

(1) For incident light and diffracted light, if the wave vector has a positive component of x in the coordinate system, its corresponding angle is positive; otherwise, it is negative.

(2) The diffraction order on the right side of the zero order is positive and the left is negative.

The optical path difference (OPD) produced by the groove error is given as

$$\boldsymbol{\xi} = \boldsymbol{\delta}_{nm}\cdot(\sin\theta_i - \sin\theta_k), \tag{11}$$

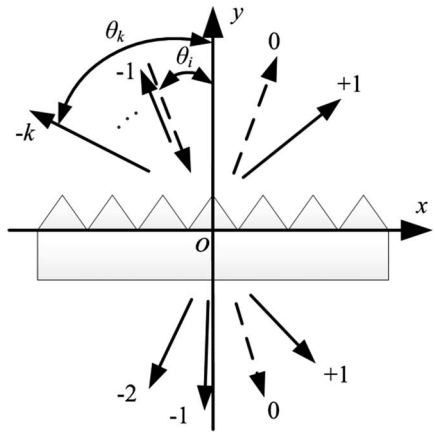

Fig. 5. Schematic diagram of sign conventions for the angles and diffraction orders.

where θ_i is the angle of incidence and θ_k is the diffraction angle of the kth diffraction order.

The grating diffraction equation is given as follows:

$$d \cdot (\sin\theta_i - \sin\theta_k) = -k \cdot \lambda, \tag{12}$$

where k is the diffraction order and λ is the wavelength of the incident light.

Equations (10)–(12) can be combined such that the diffraction wavefront of the grating, which is caused by the cosine error, can be written as

$$\Delta(k) = \boldsymbol{\delta}_{nm} \cdot \frac{-k\lambda}{d}. \tag{13}$$

From Eq. (4), the difference between the cosine errors at the two measuring beam positions can be given as

$$\Delta\zeta = \zeta_1 - \zeta_2 = \frac{2 \cdot \Delta\alpha \cdot \alpha_2 + (\Delta\alpha)^2}{2} \cdot d, \tag{14}$$

where $\Delta\alpha$ ($\Delta\alpha = \alpha_1 - \alpha_2$) is the difference between the two cosine error angles at the two measurement beam positions.

Using a combination of Eqs. (13) and (14), the diffraction wavefront of the grating that is caused by the cosine error can be written as

$$\Delta(k) = \frac{-k\lambda}{d} \cdot \boldsymbol{\delta}_{nm} = \frac{-k\lambda}{d} \cdot \begin{bmatrix} 0 & \zeta_2 & \cdots & (n-1)\cdot\zeta_2 \\ 0 & \zeta_2 + \frac{\Delta\zeta}{m-1} & \cdots & \zeta_2 + (n-1)\cdot\frac{\Delta\zeta}{m-1} \\ \vdots & \vdots & \vdots & \vdots \\ 0 & \zeta_2 + \frac{\Delta\zeta}{m-1}\cdot(j-1) & \cdots & \zeta_2 + (n-1)\cdot\frac{\Delta\zeta}{m-1}\cdot(j-1) \\ \vdots & \vdots & \vdots & \vdots \\ 0 & \zeta_2 + \frac{\Delta\zeta}{m-1}\cdot(m-1) & \cdots & \zeta_2 + (n-1)\cdot\frac{\Delta\zeta}{m-1}\cdot(m-1) \end{bmatrix}. \tag{15}$$

Fig. 6. Results of simulation of the interference fringe caused by the cosine error before cosine error correction.

From Eqs. (14) and (15), we obtain the following conclusions:

(1) If $\Delta\alpha = 0$, the cosine error does not affect the grating's diffraction wavefront;

(2) if $\Delta\alpha \neq 0$ and α_2 is a constant, the change in the diffraction wavefront is the same as the trend in $\Delta\alpha$.

The type of the interference fringe of a grating with a groove error is given as follows:

$$I = A \cdot \left[1 + \cos\left(\frac{2\pi}{\lambda} \cdot \Delta\right)\right], \tag{16}$$

where A is the light intensity coefficient.

Using a combination of Eqs. (15) and (16), the relationship between the cosine error and the interference fringes can be obtained in the form of the following matrix:

$$I = A \cdot \left\{1 + \cos\left(\frac{2\pi k}{d} \cdot \begin{bmatrix} 0 & \zeta_2 & \cdots & (n-1)\cdot\zeta_2 \\ 0 & \zeta_2 + \frac{\Delta\zeta}{m-1} & \cdots & \zeta_2 + (n-1)\cdot\frac{\Delta\zeta}{m} \\ \vdots & \vdots & \cdots & \vdots \\ 0 & \zeta_2 + \frac{\Delta\zeta}{m-1}\cdot(j-1) & \cdots & \zeta_2 + (n-1)\cdot\frac{\Delta\zeta}{m}\cdot(j-1) \\ \vdots & \vdots & \cdots & \vdots \\ 0 & \zeta_2 + \frac{\Delta\zeta}{m-1}\cdot(m-1) & \cdots & \zeta_2 + (n-1)\cdot\frac{\Delta\zeta}{m}\cdot(m-1) \end{bmatrix}\right)\right\}. \tag{17}$$

If we assume that $\alpha_1 = 0$, then the deviation of the center of the beam 2 spot during a 680 mm traverse is found to be 1.5 mm, and the cosine error angle can then be calculated to be 0.1264°. If an echelle grating with dimensions of 400 mm × 500 mm, a blazed order of −36, and a groove density of 79 grooves/mm is ruled in this case, then the peak-to-valley (PV) value of the diffraction wavefront difference caused by the cosine error according to Eq. (15) is calculated to be 3.46λ (where $\lambda = 632.8$ nm). The results of simulation of the interference fringe caused by the cosine error based on Eq. (17) are shown in Fig. 6.

From the analysis above, the beam path of the existing measurement system is prone to production of different cosine errors; this means that it will be easy to cause a new fan error

when the cosine errors of the two measurement beams are different, and we must therefore reduce the effects of the different cosine errors.

4. CORRECTION OF THE COSINE ERROR

Ideally, we would expect the cosine error angles of both measurement beams to be zero, but this scenario is actually impossible to achieve. According to the analysis given in Section 3, if the cosine error angle of the two measuring beams is not zero, we can then reduce the influence of the cosine error on grating performance by making the difference between the two cosine error angles zero. Based on these ideas, we replaced the two measuring mirrors that were located in the original beam path with a single measuring mirror; the resulting improved beam path structure for the measurement system is shown in Fig. 7.

The flatness of the measurement plane of the 450 mm × 100 mm × 50 mm measuring mirror, which was formed using a microcrystalline material with low thermal expansion, is better than $1/8\lambda$ (at 632.8 nm). Considering the following bad situation, in which we assume that $\alpha_1 = 0$, the slope at the beam 2 spot position on the plane mirror is the highest, and the angle between the cosine angles of the two beams can then be written as

$$\Delta\alpha = \alpha_1 - \alpha_2 = 0 - \arctan\left(\frac{\lambda}{8}\cdot\frac{1}{3\times 10^6}\right) = -0.00151^\circ. \tag{18}$$

If an echelle grating with dimensions of 400 mm × 500 mm, a blazed order of −36, and a groove density of 79 grooves/mm is ruled in this case, the PV value of the diffraction wavefront difference caused by the cosine error based on Eq. (15) is calculated to be $4.938\times 10^{-4}\lambda$ (where $\lambda = 632.8$ nm); the interference fringe simulation results that were caused by the cosine error in accordance with Eq. (17) are shown in Fig. 8.

From the analysis above, the PV value of the diffraction wavefront of an echelle with dimensions of 400 mm × 500 mm, a blazed order of −36, and a groove density of 79 grooves/mm was reduced from 3.46λ to $4\ .938\times 10^{-4}\lambda$

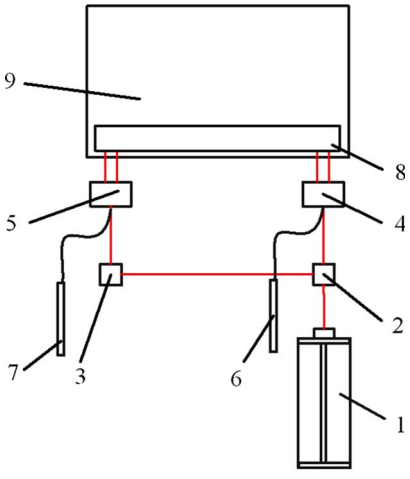

Fig. 7. Improved beam path structure for the measurement system. 1, laser; 2, beam splitter; 3, beam bender; 4, interferometer A; 5, interferometer B; 6, receptor A; 7, receptor B; 8, mirror; 9, insider carriage.

Fig. 8. Results of simulation of the interference fringe caused by the cosine error after cosine error correction.

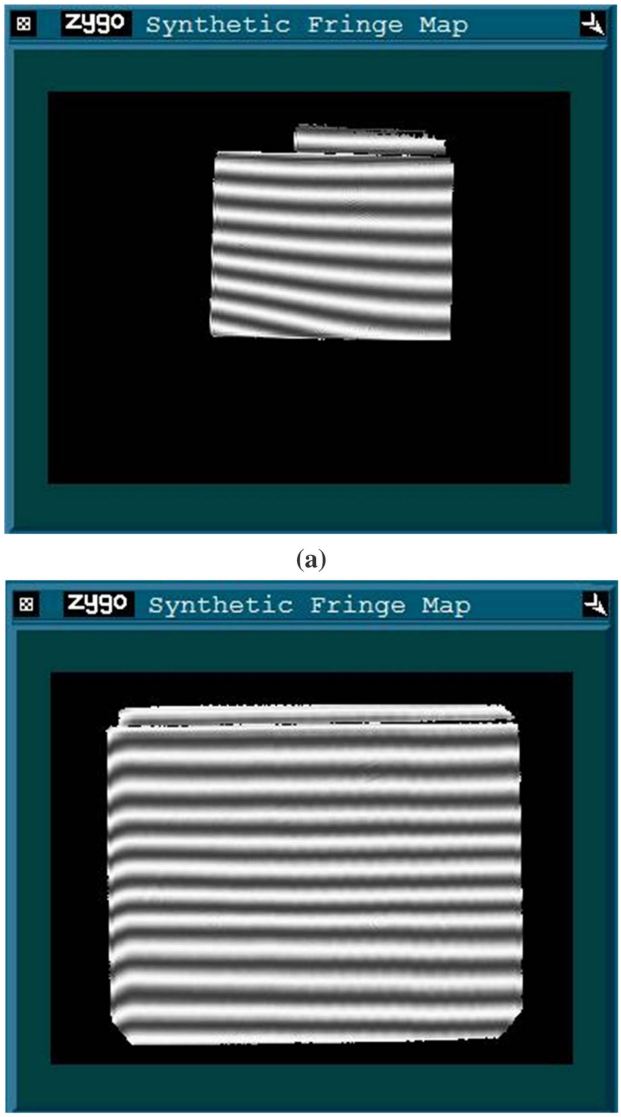

Fig. 9. Wavefront quality of echelle gratings with density of 79 grooves/mm for comparison experiment as measured using Zygo interferometer. (a) Without cosine error correction and (b) with cosine error correction.

(where $\lambda = 632.8$ nm). Comparison of Fig. 6 with Fig. 8 shows that the fan error of the grating interference fringe that was caused by the cosine error improved significantly after cosine error correction.

5. GRATING RULING EXPERIMENT

Before correction of the beam path structure, the grating wavefront constantly contains interference fringes similar to the fan pattern shown in Fig. 9(a). The echelle grating shown in Fig. 9(a) with the density of 79 grooves/mm has dimensions of 90 mm × 140 mm × 30 mm. The PV value of the wavefront difference of the blazed order (–36 th) is 0.31λ.

As shown in Fig. 9(b), after correction of the beam path structure, the interference fringe fan of the grating with density of 79 grooves/mm and dimensions of 150 mm × 240 mm has improved significantly. The PV value of the wavefront difference of the blazed order (–36th) is 0.19λ, except at the left end, where the diamond was both dropping and accelerating.

Comparison of Fig. 9(a) with Fig. 9(b) demonstrates that the proposed method reduces the effect of the cosine error on the grating performance quite effectively.

6. CONCLUSIONS

Using the beam path structure of the CIOMP-6 ruling engine, we analyzed the effects of the cosine error on grating performance, and the following conclusions were obtained.

(1) If the cosine error angles $\alpha_1 = \alpha_2$, the cosine error does not affect the diffraction wavefront of the grating and only affects the grating density, thus having little effect on grating performance.

(2) If $\alpha_1 \neq \alpha_2$, the beam path structure before correction is prone to different cosine errors, and these cosine errors will cause a fan error in the interference fringes, which means that the wavefront quality of the grating will deteriorate.

We therefore proposed a suitable correction method for the cosine error and verified the effectiveness of the proposed method through simulations and experiments.

Funding. National Basic Research Program of China (2014CB049500); National Natural Science Foundation of China (NSFC) (61505204, 61605204); Ministry of Science and Technology of the People's Republic of China (MOST) (2016YFF0102006, 2016YFF0103304).

REFERENCES

1. X. T. Li, H. L. Yu, X. D. Qi, S. L. Feng, J. C. Chu, S. W. Zhang, Jirigalantu, and Y. G. Tang, "300 mm ruling machine producing gratings and echelles under interferometric control in China," Appl. Opt. **54**, 1819–1826 (2015).
2. Jirigalantu, X. T. Li, S. W. Zhang, X. T. Mi, J. X. Gao, Bayanheshig, X. D. Qi, and Y. G. Tang, "Ruling of echelles and gratings with a diamond tool by the torque equilibrium method," Appl. Opt. **55**, 8082–8088 (2016).
3. R. Kammel, R. Ackermann, J. Thomas, J. Götte, S. Skupin, A. Tunnermann, and S. Nolte, "Enhancing precision in fs-laser material processing by simultaneous spatial, and temporal focusing," Light Sci. Appl. **3**, e169 (2014).
4. C.-H. Chang, Y. Zhao, R. K. Heilmann, and M. L. Schattenburg, "Fabrication of 50 nm period gratings with multilevel interference lithography," Opt. Lett. **33**, 1572–1573 (2008).
5. S. W. Zhang, X. T. Mi, Q. Zhang, Jirigalantu, S. L. Feng, H. L. Yu, and X. D. Qi, "Groove shape characteristics of echelle gratings with high diffraction efficiency," Opt. Commun. **387**, 401–404 (2017).
6. D. Nevejans, E. Neefs, E. Van Ransbeeck, S. Berkenbosch, R. Clairquin, L. De Vos, W. Moelans, S. Glorieux, A. Baeke, O. Korablev, I. Vinogradov, Y. Kalinnikov, B. Bach, J.-P. Dubois, and E. Villard, "Compact high-resolution spaceborne echelle grating spectrometer with acousto-optical tunable filter based order sorting for the infrared domain from 2.2 to 4.3 μm," Appl. Opt. **45**, 5191–5206 (2006).
7. H. Yang, Z. Li, X. Wang, Z. Shen, J. Gao, and S. Zhang, "Radial-quality uniformity investigations of large-area thick Al films," Opt. Eng. **54**, 045106 (2015).
8. E. Leibhardt, "Improved method for lapping a dividing gear for a ruling machine," J. Opt. Soc. Am. **42**, 447–450 (1952).
9. J. Strong, "New Johns Hopkins ruling machine," J. Opt. Soc. Am. **41**, 3–14 (1951).
10. C. Yang, X. T. Li, H. L. Yu, H. Z. Yu, J. W. Zhu, S. W. Zhang, J. X. Gao, Bayinheshig, and Y. G. Tang, "Practical method study on correcting yaw error of 500 mm grating blank carriage in real time," Appl. Opt. **54**, 4084–4088 (2015).
11. H. L. Yu, X. T. Li, J. W. Zhu, H. Z. Yu, X. D. Qi, and S. L. Feng, "Reducing the line curvature error of mechanically ruled gratings by interferometric control," Appl. Phys. B **117**, 279–286 (2014).
12. C. Yang, H. L. Yu, X. T. Li, J. W. Zhu, H. Z. Yu, Bayinheshig, X. D. Qi, and Y. G. Tang, "Real-time monitoring of ruling grating resolution by digital wavefront," Appl. Opt. **54**, 492–497 (2015).
13. X. Yao, J. Cui, H. Yu, X. Qi, X. Mi, Y. Jiang, M. Wang, and X. Li, "An improved accuracy-measuring method in manufacturing the lead screw of grating ruling machine," Precis. Eng. **49**, 344–353 (2017).
14. X. Mi, H. Yu, H. Yu, S. Zhang, X. Li, X. Yao, X. Qi, Bayanheshig, and Q. Wan, "Correcting groove error in gratings ruled on a 500-mm ruling machine using interferometric control," Appl. Opt. **56**, 5857–5864 (2017).
15. Z. Li, J. Gao, H. Yang, T. Wang, and X. Wang, "Roughness reduction of large-area high-quality thick Al films for echelle gratings by multi-step deposition method," Opt. Express **23**, 23738–23747 (2015).
16. G. R. Harrison and G. W. Stroke, "Interferometric control of grating ruling with continuous carriage advance," J. Opt. Soc. Am. **45**, 112–121 (1955).
17. G. R. Harrison, N. Sturgis, S. P. Davis, and Y. Yamada, "Interferometric calibration of precision screws and control of ruling machines," J. Opt. Soc. Am. **41**, 495–503 (1951).
18. G. R. Harrison, S. W. Thompson, H. Kazukonis, and J. R. Connell, "750-mm ruling machine producing large gratings and echelles," J. Opt. Soc. Am. **62**, 751–756 (1972).
19. T. Kita and T. Harada, "Ruling machine using a piezoelectric device for large and high-groove density gratings," Appl. Opt. **31**, 1399–1406 (1992).